Desalination and Water Treatment
www.deswater.com

doi: 10.5004/dwt.2020.25783

193 (2020) 266–273
July

Synthesizing "sulfonated styrene-divinylbenzene polymer/Fe" nanocomposite for adsorption of Mn(II) and Zn(II) ions from the waste of alkaline battery recycling factories: kinetic, thermodynamic, and isotherm adsorption studies

Vahid Hadadi

Department of Chemistry, Islamshahr Branch, Islamic Azad University, Islamshahr, Iran, Tel. +98 938659545; email: Hadadivahid57@gmail.com (V. Hadadi)

Received 29 September 2019; Accepted 5 March 2020

ABSTRACT

Recycling of alkaline batteries releases toxic and life-threatening ions to the environment. Different methods were studied to eliminate these pollutants from wastewaters. In this study, for the first time, a novel and high porous iron nanocomposite with the sulfonated styrene-divinylbenzene polymer was synthesized and was applied to eliminate Mn and Zn ions from wastewater of battery recycling factories. Fourier transform infrared and scanning electron microscope showed that a porous nanocomposite with an iron particle size of less than 100 nm was prepared. Subsequently, synthesized nanocomposite was used for adsorption of Mn and Zn ions. After optimizing adsorption parameters with standard solutions, the optimized parameters were applied for kinetic, thermodynamic, and isotherm adsorption study of real wastewater. The adsorption kinetics was modeled by first and second-order rate models and the results indicate that the second-order kinetics model was well-suited to model the kinetic adsorption of Zn and Mn ions. The thermodynamic study illustrated a spontaneous and endothermic adsorption process for both Mn and Zn ions. Isotherm studies indicated reasonable compatibility of the Freundlich model with adsorption of zinc ions. However, the Langmuir model was compatible with manganese adsorption. Consequently, synthesized nanocomposite showed reasonable characteristics for adsorption of zinc and manganese from wastewater.

Keywords: Wastewater treatment; Alkaline battery recycling factory; Polymer nanocomposite; Sulfonated styrene-divinylbenzene; Adsorption isotherms; Thermodynamic study

1. Introduction

Battery recycling factories release different heavy metal to wastewaters due to the battery washing or recycling process. Around 70% of alkaline batteries are valuable metals such as steel, zinc, and manganese. The black slag residue of the recycling process is rich in zinc and manganese that leaks to wastewaters [1]. Different methods were suggested for removing these toxic metals from the environment. Filtration, coagulation, adsorption, reverse osmosis, oxidation, ion exchange, and chemical precipitation were old fashion techniques for removing heavy metal ions from water and soil [2]. Most of these methods were costly and time consuming with low efficiency. However, the number of these techniques like coagulation and precipitation are still used in most factories. In recent years, adsorption methods are widely used because it is cost-effective and simple. Numerous materials can be used as adsorbents to remove heavy metal ions from the water. Nanomaterials were presented as the best adsorbents because of their large specific surface area [3]. Metal nanoparticle adsorbents were suggested for removing organic and inorganic pollutants [4]. Iron nanoparticles because of quick reaction and high yield in removing metal ions were studied [5]. Also, the characterization of new adsorbent containing iron chloride hydroxide nanocrystal (akaganeite)

for As(v) elimination was investigated by Deliyanni et al. [6]. Metal oxide nanoparticles like hydrous titanium dioxide as potential sorbent was used for the removal of manganese from water [7]. The thermodynamic study showed that the adsorption of manganese on titanium dioxide was spontaneous and exothermic. Moreover, it was defined that adsorption of manganese followed Langmuir adsorption isotherm. Also, oxidized multiwalled carbon nanotubes (MWCNTs) were applied for the removal of manganese from aqueous solution [8]. This investigation revealed that adsorption of manganese onto this adsorbent was spontaneous and endothermic. Second-order kinetics of reactions and following Langmuir isotherm were other results of this study. The application of isotherm, kinetics, and thermodynamic models for the adsorption of other ions like nitrate by graphene were considered [9]. Adsorption mechanisms and related isotherm of other heavy metals such as Zn ions onto carbon nano-tube multiwall were widely studied by Taghdir et al. [10]. They found that the capacity of metal ion adsorption for MWCNTs is 3 or 4 times higher than carbon active. Accordingly, Sadegh et al. [11] studied a high adsorption capacity of magnetic carbon nanotube (CNT) composite for removing Hg(II). A new method consists of its thermodynamic, kinetic, and isotherm studies were suggested for the elimination of manganese from water by electrocoagulation method [12]. Simultaneous removal of Co, Cu, Cr, and arsenate were discussed by the electrocoagulation method as well [13,14]. By polymer development, the polymeric adsorbents emerged in terms of their vast surface area, adjustable surface chemistry, perfect mechanical rigidity, and pore size distribution [15]. CNT coated by poly-amidoamine dendrimer (PAMAM) was studied as an adsorbent for adsorption of As^{3+}, Co^{2+}, and Zn^{2+} from aqueous solution [16]. Recently, nanocomposite materials were developed to remove heavy metal ions from wastewater [17]. Nanocomposite materials displayed better adsorption capacities, granulometric properties, chemical and thermal stabilities, reproducibility, and better selectivity compared to nanoparticles and CNTs [18]. The polymer nanocomposites (PNCs) because of easy preparation, cost-effective, environmental stability, large surface area, and pore volume were evaluated among nanocomposites [19–22]. Magnetite-carbon nanocomposites were studied for the removal of metal ions from aqueous solutions [23]. The magnetite-bentonite nanocomposite was used for the elimination of Ni^{2+}, Cu^{2+}, Cd^{2+}, and Zn^{2+} ions from an affluent [24]. In another study, magnetic Fe_3O_4 nanoparticles were synthesized and its surface was modified with 3-aminopropyl trimethoxysilane for adsorption of Co^{2+}, Cr^{3+}, Zn^{2+}, and Cd^{2+} [25]. Also, Magnetic carbon-coated Fe_3O_4 microspheres activated with 1-ethyl-3-(3-dimethyl aminopropyl)-carbodiimide hydrochloride were discussed to adsorb bovine serum albumin [26]. A novel PNC adsorbent such as sulfonated styrene-divinylbenzene and iron was studied for adsorption of cadmium ions [27].

In summary, it is clear that increases in surface area and porosity of PNC increases the contact area of adsorbent with metal. So, synthesizing higher porous nanocomposite leads to the evolution of adsorption capacity. Since the poly sulfonated styrene-divinylbenzene is a porous polymer, it was used as a base for synthesizing the iron PNC adsorbent in this study. On the other side, the elimination of toxic metal like Zn and Mn from wastewater of battery recycling factories by PNCs wasn't investigated yet. Then, the sulfonated styrene-divinylbenzene polymer/Fe nanocomposite was used for adsorption of Mn(II) and Zn(II) from the wastewater of the alkaline battery recycling factory. Adsorption parameters like contact time, pH, PNC dosage, kinetic, thermodynamic behaviors, etc. were investigated. Finally, Langmuir, Freundlich, and Temkin adsorption isotherm models were applied to fit the experimental data. The novelty of this investigation was applying a novel and high porous iron nanocomposite for removal of Mn and Zn ions from the wastewater of recycling alkaline battery factories.

2. Materials and methods

2.1. Materials, apparatuses, and equations

- The wastewater consists of Zn^{2+} (34 ppm) and Mn^{2+} (28 ppm) were collected from Peyman Recycling factory.
- All chemical reagents were supplied by Fluka and Merck. A stock solution of Mn(II) and Zn(II) ion with an initial concentration of 30 ppm was prepared by using $(Mn(NO_3)_2{\cdot}4H_2O$ and $(Zn(NO_3)_2{\cdot}4H_2O)$ salts with purity above 97%.
- A Fourier transform infrared (FT-IR) spectrometer (Jasco, FT-IR 420) in transmission mode under dry nitrogen flow (10 cm^3 per minute) was used.
- A scanning electron microscope (SEM, JEOL field emission scanning electron microscope, JSM-6700F) was used for morphology investigation.
- Adsorbent and specimens were shaken in an ultrasonic bath Model S 80H, Elmasonic Co.
- The equilibrium concentrations of metal ions were determined by atomic absorption spectrophotometer (Model AA220, Varian Co., USA).
- The adsorbed metal ions concentration was obtained using Eq. (1):

$$q_e = \frac{\left(C_0 - C_e\right)V}{m} \tag{1}$$

where q_e is the equilibrium uptake (mg g^{-1}) of adsorbate, C_0 is the initial ion concentration (mg L^{-1}), C_e is the equilibrium ion concentration (mg L^{-1}), V and m are the volume of the solution (L), and the adsorbent mass (g), respectively.

- The adsorption percentages were calculated by the following equation:

$$\text{Adsorption}\% = \left(\frac{C_0 - C_e}{C_0}\right) \times 100 \tag{2}$$

2.2. Polymer nanocomposite preparation

PNC was prepared by mixing 1 g of poly sulfonated styrene-divinylbenzene and benzol peroxide (as a cross-linked agent) to 300 mL of ethanol and $FeCl_2{\cdot}4H_2O$ (0.4 M) solution. Then, $NaBH_4$ solution (1 M) was added and was stirred for 20 min. The synthesized PNC was collected from

the solution and was washed thrice with isopropanol to prevent oxidation of nanoparticles in PNC (Fig. 1).

2.3. Determination of adsorption percentages

The required dosages of PNCs were added to Mn and Zn ions solutions and were mixed in an ultrasonic bath under the adjusted time and temperature. The PNC was separated from the solution by centrifuging and filtration. Finally, the concentrations of unadsorbed metal ions and their percentages were determined by atomic absorption and Eq. (2).

3. Results and discussion

3.1. PNC characteristics

The morphology of synthesized PNC was investigated with SEM and is presented in Fig. 2. The morphology study showed that the spherical nanoparticles were distributed in uniform size (less than 100 nm) in PNC. According to the SEM picture, too many holes were created by this polymer that made a high porous PNC with a high surface.

Also, FT-IR was used to consider the physicochemical interactions between the polymer and iron nanoparticles. In order to see the stretching vibration of iron, the iron particles in PNC were converted to the iron oxide by contacting PNC with water and oxygen for 48 h. Only the polysulfonated styrene-divinylbenzene (PSD) was contacted with water and oxygen in the same condition as reference. The FT-IR spectrum of iron oxide particles, PSD, and PNC are presented in Figs. 3a–c, respectively. Fig. 3a showed a stretching vibration peak of iron oxide in about 600 cm^{-1}. On the other side, a comparison between the PSD spectrum (Fig. 3b) and the PNC (Fig. 3c) showed a peak related to Iron oxide particles in the range of 600–500 cm^{-1} for PNC. This wide and strong peak proved that iron nanocomposite was prepared in PSD.

Obtained data from SEM and FT-IR of PNC showed that porous iron nanocomposite with a size of less than 100 nm were synthesized.

Subsequently, in the next step, the synthesized PNC was used for consideration of effective adsorption parameters of Zn and Mn ions.

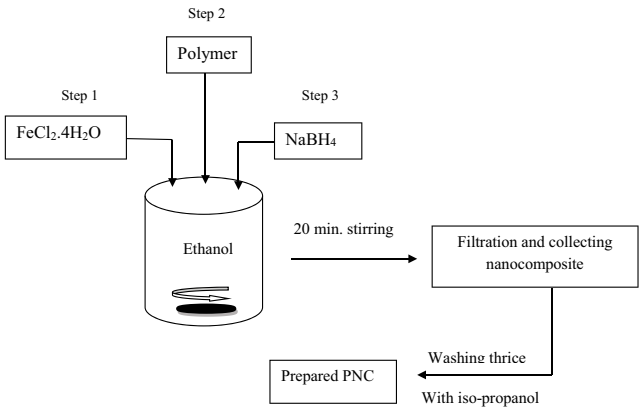

Fig. 1. PNC preparation flowchart.

3.2. Effect of contact time

Since contact time is one of the most important factors in adsorption value, contact time between the adsorbate and adsorbent were studied. The optimum contact time was calculated by mixing 25 mg of PNCs with 10 mL of Mn(II) and 10 mL of Zn(II) solutions with an initial concentration of 30 mg L^{-1} in separate beakers. The mixing process continued for 5–60 min and the adsorption percentage of Mn and Zn ions were determined from time to time according to section 2.3 (determination of adsorption percentages). Extracted results are plotted in Fig. 4. Evidence showed that the best contact time for Mn and Zn ions was about 5 and 10 min, respectively.

3.3. Effect of pH

To estimating optimum pH, 25 mg of PNCs were mixed with 10 mL of Mn(II) and 10 mL of Zn(II) solutions with an initial concentration of 30 mg L^{-1}. Then in different pHs from 3 to 11 and at optimum contact time (5 min for Mn(II) and 10 min for Zn(II)) adsorptions were determined (Fig. 5). Optimum pHs for Mn(II) and Zn(II) adsorption were calculated in pH = 7 and 9, respectively.

3.4. Effect of adsorbent dosage

The different values of adsorbent were added to 10 mL of Mn(II) and 10 mL of Zn(II) solutions with a concentration of 30 mg L^{-1} to optimize dosages of adsorbent (Fig. 6).

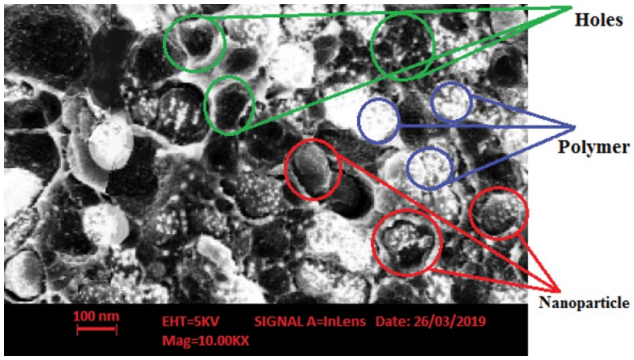

Fig. 2. SEM of synthesized PNC.

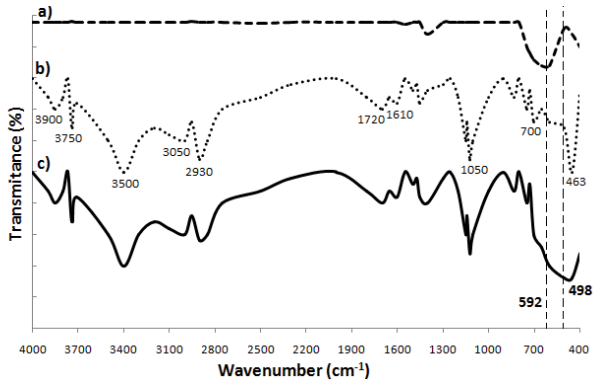

Fig. 3. FT-IR spectrums of (a) iron oxide, (b) only polysulfonated styrene-divinylbenzene, and (c) PNC.

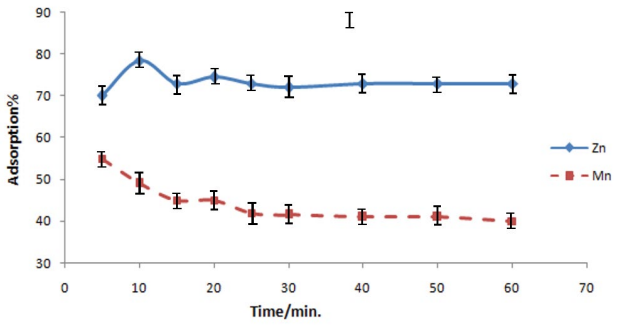

Fig. 4. Effect of contact time on adsorption of Mn and Zn ions onto the PNC.

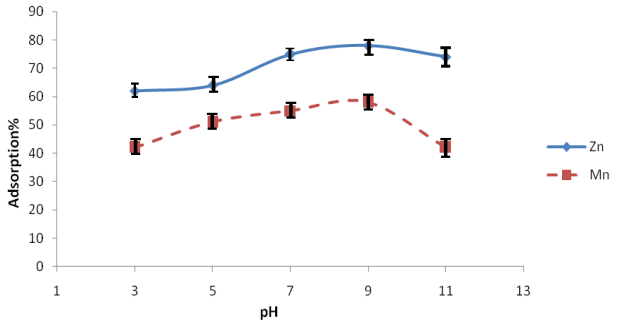

Fig. 5. Effect of pH on the adsorption of Mn(II) and Zn(II) onto the PNCs.

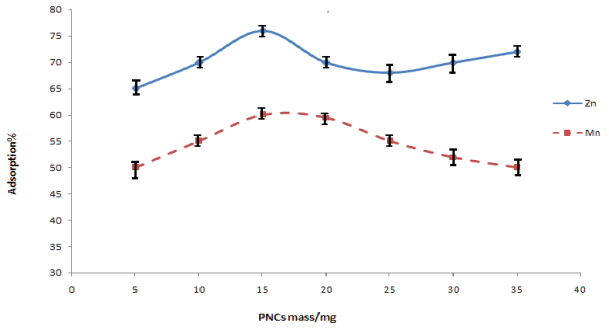

Fig. 6. Effect of the dosage of PNCs on the adsorption percentage of Mn(II) and Zn(II) from aqueous solution.

Normally, an increase in adsorbent concentration should lead to rising in adsorption percentage. However, Fig. 6 shows a decreasing in adsorption value in more than 15 mass/mg of PNC for both Mn(II) and Zn(II) ions. Diminish in adsorption in the high concentration of absorbent was due to an aggregation of absorbent particles. Thus, 15 mg of PNC was selected as an optimum adsorbent dosage for both ions.

3.5. Kinetic study

In order to consider the kinetics of Mn and Zn adsorption over the PNC, the adsorption kinetics was investigated by first-order and second-order kinetic models. Two pseudo-first-order and pseudo-second-order models were tested to obtain the rate constants and adsorption mechanism.

3.5.1. First-order model

The first-order model generally explains as Eq. (3):

$$\log\left(q_e - q_t\right) = \log\left(q_e\right) - \left(\frac{k_1}{2.303}\right)t \tag{3}$$

where q_e is adsorption capacities at equilibrium and q_t is adsorption capacities at time t (min), k_1 (min^{-1}) is the rate constant of the first-order adsorption. The plot of $\log(q_e - q_t)$ vs. t gives the linear relationship in which k_1 and q_e can be determined by the slope and intercept, respectively. The results of kinetic adsorption of Mn and Zn according to the first-order equation are plotted in Fig. 7. The k_1 for Mn and Zn was estimated at 0.201 and 0.219, respectively. The poor correlation coefficient (less than 0.987) proved that the kinetic of ions was not fitted with the first-order model.

3.5.2. Second-order model

Second-order kinetic model is expressed as Eq. (4):

$$\frac{t}{q_t} = \frac{1}{k_2 q_e^2} + \frac{t}{q_e} \tag{4}$$

where k_2 is the rate constant of second-order adsorption that is calculated from the slope of the straight line. Fig. 8 presents the t/q_t variation vs. t for both Mn and Zn adsorption onto PNC. The rate constants (k_2) for Mn and Zn were calculated 0.008 and 0.09, respectively. The kinetic data such as a good correlation coefficient (more than 0.997) for both ions indicated that the adsorption process was controlled by the pseudo-second-order equation.

3.6. Thermodynamic behavior and the effect of temperature on real sample

To understand the effect of temperature on the adsorption process, thermodynamic parameters were determined at various temperatures. So, a real sample in optimized conditions (pH, contact time, and adsorbent dosage) was used for the thermodynamic study. But in additional processes, some interference substances were precipitated by controlling pH between 7 and 9. The sediments were separated from the solution by centrifuging and filtration. In the next step, the residue solution was separated into two parts. In one part, 15 mg of PSD (polysulfonated styrene-divinylbenzene alone) was added as a reference and in the next part, 15 mg of PNC was added. Then, the adsorption of Zn and Mn ions was studied in optimized conditions at different temperatures (25°C, 40°C, 50°C, 55°C, and 65°C). The adsorption results onto PNC and PSD are presented in Fig. 9 and Table 1, respectively. The data in Table 1 showed that adsorption of Mn and Zn ions onto polymer alone was negligible and it was ignored.

Note that the adsorption process in wastewater was performed in two beakers, once in pH = 7 for adsorption of Mn and once in pH = 9 for adsorption of Zn. According to Fig. 9, the adsorption increased at higher temperatures

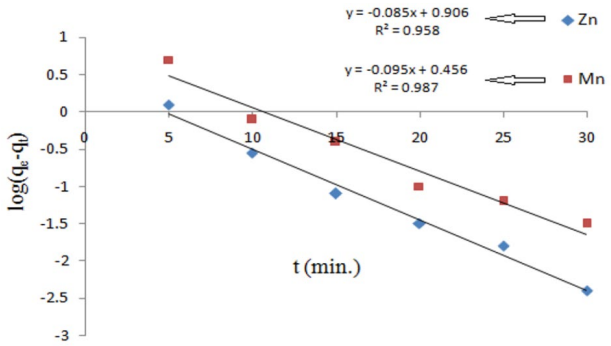

Fig. 7. Adsorption kinetics of Mn and Zn ions by PNC for pseudo-first-order model.

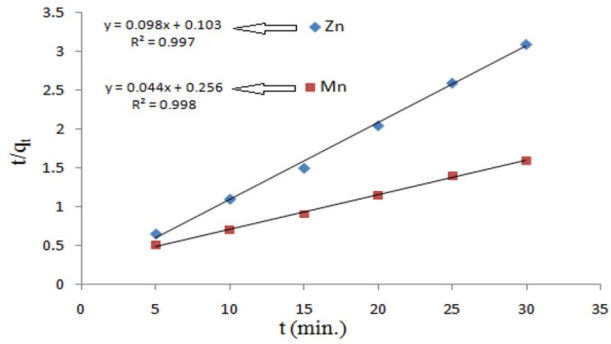

Fig. 8. Adsorption kinetics of Mn and Zn ions by PNC for pseudo-second-order model.

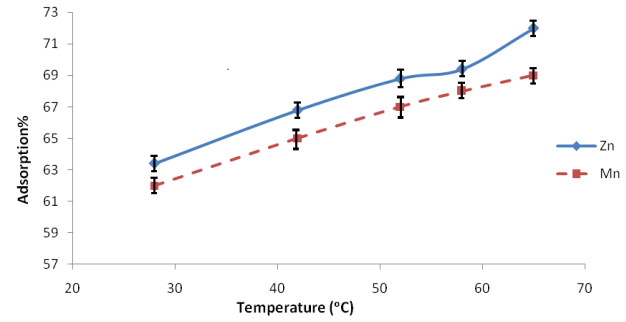

Fig. 9. Effect of the temperature on the adsorption of Mn(II) and Zn(II) onto PNC.

for both Mn and Zn ions. Comparison between Fig. 6 (adsorption of Zn and Mn lonely at 25°C) and Fig. 9 (adsorption of Zn and Mn ions together in a real sample at 25°C) showed that adsorption of Zn ions decreased in the presence of Mn. However, adsorption of Mn(II) was independent of Zn ions in solution.

In the aim of explaining the thermodynamic behavior of the real sample, thermodynamic parameters like enthalpy, entropy, and Gibbs free energies are extracted from Fig. 9. Subsequently, enthalpy changes ($\Delta H°$) and entropy changes ($\Delta S°$) were calculated by the Van't Hoff equation:

$$\ln K_L = \frac{\Delta S°}{R} - \frac{\Delta H°}{R}\frac{1}{T} \quad (5)$$

Table 1
Effect of the temperature on the adsorption of Zn and Mn ions onto the PSD

Temperature (°C)	Zn adsorption (%)	Mn adsorption (%)
28	1	0.9
42	1.02	1.04
52	1.1	1.1
58	1.13	1.1
65	1.2	1.18

where K_L was given from the division of q_e on C_e and R was the ideal gas constant (8.314 J $mol^{-1}K^{-1}$). The Van't Hoff equation for Zn(II) and Mn(II) adsorption are shown in Figs. 10 and 11, respectively.

Also, standard enthalpy changes ($\Delta H°$) and standard entropy changes ($\Delta S°$) were extracted from the slope and intercept of the line, respectively. The results are given in Tables 2 and 3.

$\Delta G°$s were calculated by Eq. (6) and are presented in Tables 2 and 3.

$$\Delta G° = \Delta H° - T\Delta S° \quad (6)$$

The positive $\Delta H°$ in Tables 2 and 3 explained endothermic adsorption processes for both ions. In addition, positive $\Delta S°$ showed that the entropy of reactions for Mn and Zn ions was expanded in the adsorption process. Positive values of entropy change showed increase randomness of the solution interface during the adsorption of manganese and zinc ions. The evolution in adsorption capacity at higher temperatures was related to high porosity due to PNC structure. Minus $\Delta G°$ in whole temperatures discussed a spontaneous reaction between PNC and adsorption of ions. The same results were obtained by other researchers about Mn and Zn removal by different adsorbent [7,8,12].

3.7. Effect of initial ion concentrations and adsorption isotherms in the real sample

In this study, different sorption isotherms, namely, Langmuir, Freundlich, and Temkin isotherms were examined [13]. The Langmuir isotherm, which is valid for monolayer sorption onto a surface, is given by Eq. (7):

$$q_e = \frac{q_m K C_e}{\left(1 + K C_e\right)} \quad (7)$$

Generally, the Langmuir model presents in several linear forms. In this study, the linear model Eq. (8) was used.

$$\frac{1}{q_e} = \frac{1}{q_m} + \frac{1}{K q_m}\left(\frac{1}{C_e}\right) \quad (8)$$

where q_e (mg g^{-1}) was the adsorbate value that adsorbed by 1 g of adsorbent, C_e (mg L^{-1}) was the equilibrium concentration of adsorbate in the solution, q_m (mg g^{-1}) was the value of

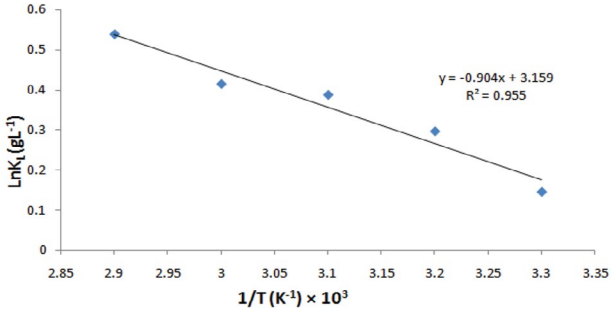

Fig. 10. Van't Hoff equation for Zn(II).

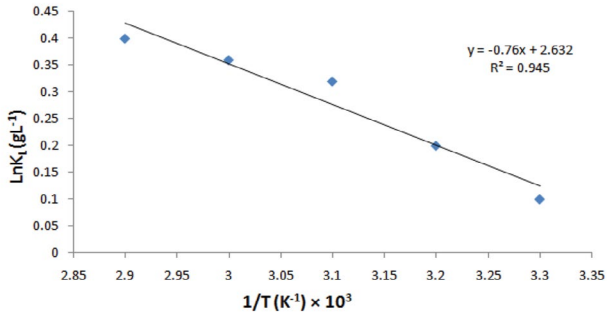

Fig. 11. Van't Hoff equation for Mn(II).

Table 2
ΔG°, ΔH°, and ΔS° for Zn ion

Temperature (K)	ΔG° (kJ/mol)	ΔH° (kJ/mol)	ΔS° (kJ/mol)
301	–400.4		
315	–768.6		
325	–1,031.6	7,515.9	26.3
331	–1,189.4		
338	–1,373.5		

Table 3
ΔG°, ΔH°, and ΔS° for Mn ion

Temperature (K)	ΔG° (kJ/mol)	ΔH° (kJ/mol)	ΔS° (kJ/mol)
301	–453.9		
315	–768.9		
325	–993.9	23,686.6	73.2
331	–1,128.9		
338	–1,286.4		

monolayer capacity of the adsorbate that adsorbed in 1 g of adsorbent, and K is the Langmuir constants.

The $1/q_e$ vs. $1/C_e$ diagrams for Zn(II) and Mn(II) ions are plotted in Figs. 12 and 13, respectively. The results should be in a straight line that its intercept represents $1/q_m$ and slope shows $1/Kq_m$. Hence, the Langmuir isotherm parameters for adsorption of Mn(II) and Zn(II) ions are presented in Table 4.

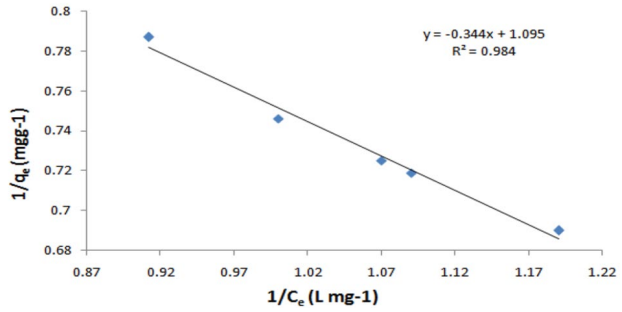

Fig. 12. Langmuir adsorption isotherm for Zn(II).

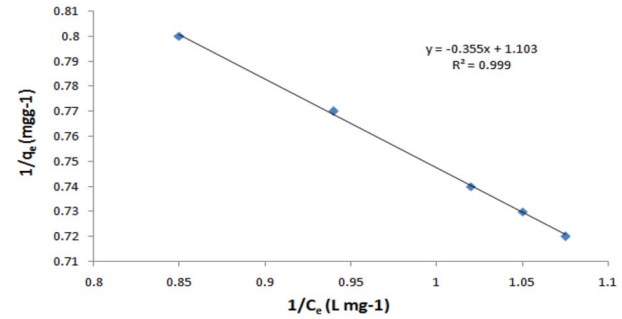

Fig. 13. Langmuir adsorption isotherm for Mn(II).

Table 4
Langmuir isotherm parameters for adsorption of Mn(II) and Zn(II) ions onto the PNC

Ion	q_m (mg g^{-1})	K (L mg^{-1})	R^2
Zn	0.913	–3.18	0.984
Mn	0.907	–3.1	0.999

Good correlation coefficients for manganese adsorption indicated the applicability of the Langmuir model. The value of q_m calculated by the Langmuir isotherm was close to the experimental value at given experimental conditions. Consequently, the manganese is adsorbed in the form of monolayer coverage on the surface of the adsorbent. This result was compatible with the results of other researchers [9,13].

The Freundlich adsorption isotherm model which is applicable for heterogeneous surfaces was analyzed as well. This model is generally valid for reversible adsorption that is not limited to monolayer adsorption. The equation is as follows:

$$q_e = k_F C_e^{1/n} \tag{9}$$

or in the logarithmic form:

$$\log q_e = \log k_F + \frac{1}{n}\log C_e \tag{10}$$

where k_F and n are the Freundlich model constants. The numerical value of $1/n$ indicates the adsorption capacity.

The results should be in a straight line that its intercept represents $\log k_F$ and slope shows $1/n$. The $1/n$ parameter is adsorption capacity and k_F is the adsorption intensity. If the n falling between 1 and 0.1 indicates favorable adsorption. The Freundlich isotherm parameters for adsorption of Mn(II) and Zn(II) ions were calculated from intercepts and slopes of Figs. 14 and 15 that were presented in Table 5. Data in Table 5 reveals that $1/n$ was less than 0.1 which proved incompatibility of the Freundlich adsorption model of these ions onto PNC.

Temkin adsorption isotherm was studied as well as Langmuir and Freundlich models. The Temkin model is generally valid for monolayer adsorption. This model is used for adsorbents with adsorption sites that are in different energy. Temkin equation and its linear form are written as follows:

$$q_e = \frac{RT}{b}\ln\left(K_T C_e\right) \tag{11}$$

$$q_e = B\ln C_e + B\ln K_T \tag{12}$$

where $B = RT/b$ is a constant related to the heat of adsorption and K_T was the constant of the Temkin model. Temkin constant and B can be calculated from the intercept and slope of the straight-line plot of q_e vs. $\ln C_e$, respectively (Figs. 16 and 17). The relative isotherm parameters for both Mn and Zn ions are shown in Table 6.

Correlation coefficients in Tables 4–6 indicated that the Temkin model was the best model for the adsorption process of Zn(II) ions. In other word, the adsorption mechanism for Zn ions onto PNC was a monolayer process with different energies in adsorption sites. While Langmuir isotherm was a fit model for adsorption of Mn ions. The obtained result described that the adsorption mechanism for Mn ions followed the monolayer process but in the same energies in adsorption sites.

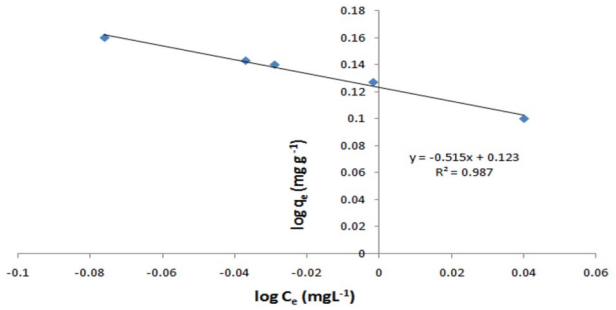

Fig. 14. Freundlich adsorption isotherm for Zn(II).

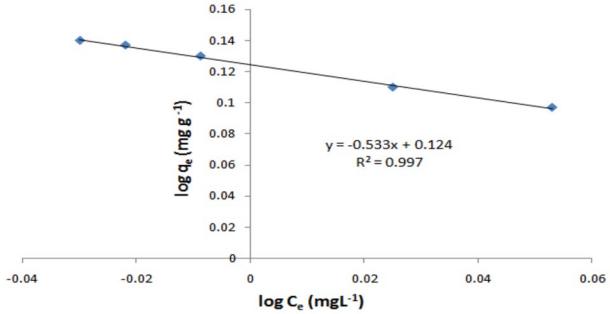

Fig. 15. Freundlich adsorption isotherm for Mn(II).

4. Conclusion

In this study, a novel polymer iron nanocomposite was synthesized. FT-IR spectrum showed that the iron nanocomposite was synthesized correctly. Also, SEM of PNC indicated a porous iron nanocomposite with particle size

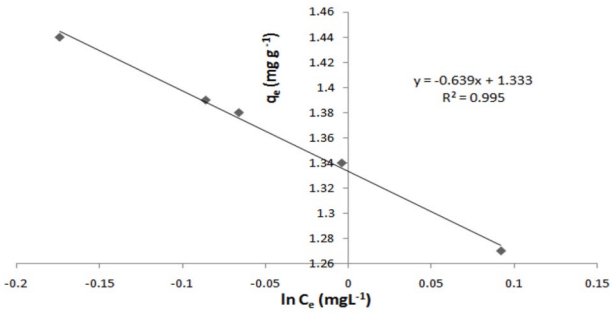

Fig. 16. Temkin adsorption isotherm for Zn(II).

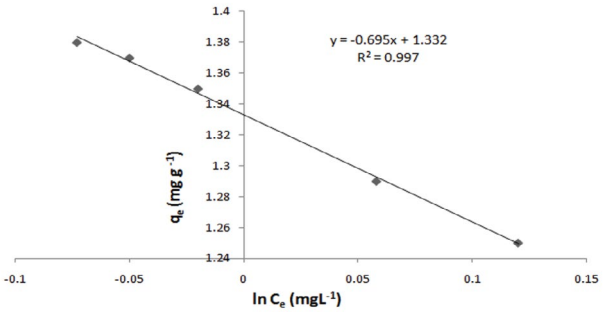

Fig. 17. Temkin adsorption isotherm for Mn(II).

Table 5
Freundlich isotherm parameters for adsorption of Mn(II) and Zn(II) ions onto the PNCs

Ion	k_F (mg g^{-1})	$1/n$	R^2
Zn	1.327	–1.94	0.987
Mn	1.33	–1.876	0.997

Table 6
Temkin isotherm parameters for adsorption of Mn(II) and Zn(II) ions onto the PNC

Ion	K_T (L g^{-1})	B_1	R^2
Zn	0.124	–0.639	0.995
Mn	0.147	–0.695	0.997

less than 100 nm was prepared. In the next experiment, PNC was used for the elimination of Mn and Zn ions from wastewater of battery recycling factories. Experimental data showed that optimum contact times for adsorption of zinc and manganese ions onto PNC were 10 and 5 min, respectively. These results proved that reasonable adsorption efficiency achieved in a short time (maximum 10 min.). Also, the optimum pHs calculated for adsorption of Zn(II) (pH = 9) and Mn(II) (pH = 7). The maximum PNC dosage for both considered ions was obtained about 15 mg. A comparison between PNC absorbents and MWCNT absorbent [10] showed that PNC absorbents were more effective for the elimination of these ions. Study on the real sample (wastewater of battery recycling factories) considered although adsorption of Zn ions decreased in presence of Mn and other ions, adsorption of Mn ions was independent of other substances in the real sample. The adsorption kinetics was modeled by first- and second-order rate models and the results indicate that the second-order kinetics model was well-suited to model the kinetic adsorption of Zn and Mn ions. The thermodynamic studies on the real sample proved a spontaneous and endothermic adsorption process for both Mn and Zn ions onto PNC. Furthermore, positive $\Delta S°$ showed that the entropy of reactions increased in the adsorption process. Isotherm's study represented that the adsorption of Zn ions onto PNC followed the Temkin model. So, the adsorption process for Zn ions was monolayer with different energy in absorbent sites. The results also showed that adsorption of Mn(II) ions onto PNC had better agreement with the Langmuir isotherm. The results of this study exhibited that synthesized nanocomposite showed good efficiency for adsorption of Zinc and Manganese from the recycling battery wastewaters.

Acknowledgments

Special thanks from Elham Taghdir for help. This research did not receive any specific grant from funding agencies in the public, commercial, or not-for-profit sectors.

References

[1] ABRI, Australian Battery Recycling Initiative, 2019. Available at: http://www.batteryrecycling.org.au/home
[2] D.W. Connell, C. Birkinshaw, T.F. Dwyer, Heavy metal adsorbents prepared from the modification of cellulose: a review, Bioresour. Technol., 99 (2008) 6709–6724.
[3] S.S. Banerjee, D.H. Chen, Fast removal of copper ions by gum arabic modified magnetic nano-adsorbent, J. Hazard. Mater., 147 (2007) 792–799.
[4] X. Chen, J.V. Wright, J.L. Conca, L.M. Peurrung, Effects of pH on heavy metal sorption on mineral apatite, Environ. Sci. Technol., 31 (1997) 624–631.
[5] J. Gao, H. Gu, B. Xu, Multifunctional magnetic nanoparticles: design, synthesis, and biomedical applications, Acc. Chem. Res., 42 (2009) 1097–1107.
[6] E. Deliyanni, D. Bakoyannakis, A. Zouboulis, K. Matis, Sorption of As(V) ions by akaganéite-type nanocrystals, Chemosphere, 50 (2003) 155–163.
[7] R. Kamaraj, P. Ganesan, S. Vasudevan, Use of hydrous titanium dioxide as potential sorbent for the removal of manganese from water, J. Electrochem. Sci. Eng., 4 (2014) 187–201.
[8] P. Ganesan, R. Kamaraj, G. Sozhan, S. Vasudevan, Oxidized multiwalled carbon nanotubes as adsorbent for the removal of manganese from aqueous solution, Environ. Sci. Pollut. Res., 20 (2013) 987–996.
[9] P. Ganesan, R. Kamaraj, S. Vasudevan, Application of isotherm, kinetic and thermodynamic models for the adsorption of nitrate ions on graphene from aqueous solution, J. Taiwan Inst. Chem. Eng., 44 (2013) 808–814.
[10] E. Taghdir, M. Aghaie, V. Hadadi, Adsorption study of Cr(III), Ni(II) and Zn(II) ions onto the multi-walledcarbon nanotubes, Russ. J. Phys. Chem. B, 9 (2015) 399–405.
[11] H. Sadegh, A. Gomaa, A.S. Hamdy Makhlouf, K.F. Chong, N.S. Alharbi, S. Agharwal, V.K. Gupta, MWCNTs-Fe_3O_4 nanocomposite for Hg(II) high adsorption efficiency, J. Mol. Liq., 258 (2018) 345–353.
[12] P. Ganesan, J. Lakshmi, G. Sozhan, S. Vasudevan, Removal of manganese from water by electrocoagulation: adsorption, kinetics and thermodynamic studies, Can. J. Chem. Eng., 91 (2013) 448–458.
[13] S. Vasudevan, J. Lakshmi, G. Sozhan, Simultaneous removal of Co, Cu, and Cr from water by electrocoagulation, Toxicol. Environ. Chem., 94 (2012) 1930–1940.
[14] S. Vasudevan, J. Lakshmi, G. Sozhan, Studies on the removal of arsenate from water through electrocoagulation using direct and alternating current, Desal. Water Treat., 48 (2012) 163–173.
[15] N.M. Mahmoodi, F. Najafi, A. Neshat, Poly(amidoamine-co-acrylic acid) copolymer: synthesis, characterization and dye removal ability, Ind. Crops Prod., 42 (2013) 119–125.
[16] B. Hayati, A. Maleki, N, Farhood, G. Fardin, M. Gordon, G. Vinod Kumar, N. Marzban, H.P. Shivaraju, Heavy metal adsorption using PAMAM/CNT nanocomposite from aqueous solution in batch and continuous fixed bed systems, Chem. Eng. J., 346 (2018) 258–270.
[17] N. Jarrah, N.D. Muazu, M. Zubair, M. Al-Harthi, Enhanced adsorptive performance of Cr(VI) onto layered double hydroxide-bentonite composite: isotherm, kinetic and thermodynamic studies, Sep. Sci. Technol., (2019) 1–13.
[18] L. Duan, H. Ning, W. Tongqing, W. Hong, L. Lixia, S. Yue, X. Xianmei, Removal of copper and lead from aqueous solution by adsorption onto cross-linked chitosan/montmorillonite nanocomposites in the presence of hydroxyl-aluminum oligomeric cations: equilibrium, kinetic, and thermodynamic studies, Chem. Eng. Commun., 203 (2016) 28–36.
[19] M. Ebadi, H. Shagholani, H. Jahangiri, High efficient nanocomposite for removal of heavy metals (Hg^{2+} and Pb^{2+}) from aqueous solution, J. Nanostruct., 6 (2016) 23–27.
[20] S. Hashemian, H. Saffari, S. Ragabion, Adsorption of Cobalt(II) from aqueous solutions by Fe_3O_4/bentonite nanocomposite, Water Air Soil Pollut., 226 (2015) 2212.
[21] S. Samadi, R. Motallebi, M. Nasiri Nasrabadi, Synthesis, characterization and application of Lanthanide metal-ion-doped TiO_2/bentonite nanocomposite for removal of Lead(II) and Cadmium(II) from aquatic media, J. Water Environ. Nanotechnol., 1 (2016) 35–44.
[22] P.K. Jaseela, J. Garvasis, A. Joseph, Selective adsorption of methylene blue (MB) dye from aqueous mixture of MB and methyl orange (MO) using mesoporous titania (TiO_2) – poly vinyl alcohol (PVA) nanocomposite, J. Mol. Liq., 286 (2019) 110908.
[23] A. Andelescu, M.A. Nistor, S.G. Muntean, M.E. Rădulescu-Grad, Adsorption studies on copper, cadmium, and zinc ion removal from aqueous solution using magnetite/carbon nanocomposites, Sep. Sci. Technol., 53 (2018) 2352–2364.
[24] M. Eskandari, M.Z. Khatir, A.K. Darban, M. Meshkini, Decreasing Ni, Cu, Cd, and Zn heavy metal using magnetite-bentonite nanocomposites and adsorption isotherm study, Mater. Res. Express, 5 (2018) 45030.
[25] A. Masoumi, M. Ghaemy, A.N. Bakht, Removal of metal ions from water using poly(MMA-*co*-MA)/modified-Fe_3O_4 magnetic nanocomposite: isotherm and kinetic study, Ind. Eng. Chem. Res., 53 (2014) 8188–8197.
[26] J. Shan, C. Kim, Z. Zhang, L. Wang, T. Sun, Adsorption of BSA on carbon-coated Fe_3O_4 microspheres activated with 1-ethyl-3-(3-dimethylaminopropyl)-carbodiimide hydrochloride, J. Wuhan Univ. Technol. Sci. Ed., 33 (2018) 1–8.
[27] J.R. Imanova, A.A. Azizov, A.M. Nabiev, F.G. Khalilova, R.M. Alosmanov, Adsorption of cadmium ions isotherm from water into polymer nanocomposite, Chem. Probl., 2018 (2018) 73–77.